

# Improved Performance of CSD-Grown $Y_{1-x}Gd_xBa_2Cu_3O_7$ -BaHfO<sub>3</sub> Nanocomposite Films on Ni5W Substrates

Pablo Cayado , Hannes Rijckaert , Thomas Thersleff, Manuela Erbe , Jens Hänisch , Isabel Van Driessche, and Bernhard Holzapfel

**Abstract**— $Y_{1-x}Gd_xBa_2Cu_3O_7$ -BaHfO<sub>3</sub> (YGBCO-BHO) nanocomposite films containing 12 mol% BHO nanoparticles and different amounts of Gd,  $x$ , were grown by Chemical Solution Deposition (CSD) on Ni5W substrates in order to investigate the impact of the rare-earth stoichiometry on the structure and superconducting properties of these films. For Gd contents  $x > 0.5$ , epitaxial YGBCO-BHO films with an approximate thickness of 270 nm self-field critical current density  $J_c$  at 77 K  $\sim 1.5$  MA/cm<sup>2</sup> were obtained. The field dependence of the critical current density  $J_c(B)$  shows a much larger accommodation field and lower exponents  $\alpha$  in  $J_c \sim B^{-\alpha}$  values compared to pristine YBCO films. This is both due to the high amount of individual nanoparticles in the matrix as observed in TEM images and the higher critical temperatures  $T_c$ . The results show that the CSD is a potential candidate for the preparation of REBCO films in long-length coated conductors.

## I. INTRODUCTION

THE fabrication of second-generation high-temperature superconducting tapes or Coated Conductors (CCs) is one most active areas in the field of superconductivity. In general, the architecture of these CCs consist of a metallic substrate, several buffer layers, the superconducting films and some protective coatings. The superconducting films in the CCs are usually made by  $REBa_2Cu_3O_7$  (REBCO, RE rare earth) compounds whose properties make them appropriate for various electric power applications [1]–[3].

The choice of the most suitable REBCO for the fabrication of the CCs is often difficult. Most of the research nowadays is devoted to  $YBa_2Cu_3O_7$  (YBCO) but there are other REBCO compounds that exhibit, in some cases, better superconducting properties [4]–[7]. Nevertheless, and despite the advantages, the

use of these alternative REBCO compounds is not as common as YBCO because their synthesis is, in general, very challenging. The size of these ions (either larger or smaller than  $Y^{3+}$ ) hinder their correct placement on the REBCO lattice decreasing drastically its stability [4], [8]–[10]. As a recent study shows, the growth temperature window systematically narrows and shifts to higher temperature for increasing difference of the ionic radius from optimum  $Y^{3+}$  [11].

The mixing of different  $RE^{3+}$  ions has appeared as attractive alternative to the complicated synthesis of the single-RE-BCO compounds while keeping the improvement in performance. The mixture of different  $RE^{3+}$  ions allows to broaden the window of suitable growth conditions, as we have recently shown in the case of the  $Y_{1-x}Gd_xBa_2Cu_3O_{7-x}$ -BaHfO<sub>3</sub> (YGBCO-BHO) films deposited on single crystal substrates [12], which ease remarkably the synthesis.

The improvement in the superconducting properties in the mixed compounds is attributed to an enhancement of the flux pinning due to the critical temperature  $T_c$  fluctuations generated by the structures associated to the substitution on the RE sites of the crystal structure. The size and properties of these structures are defined by several variables, e.g., the type and molar fraction of the substituent [13], [14]. The combination of this RE mixing with the introduction of secondary phases in the REBCO matrix, creating in this way the so called nanocomposites, can further improve the final properties of the films as we could demonstrate in our previous work [12]. The use of nanocomposites has been deeply study by multiple groups showing a large positive impact the in-field transport properties of REBCO films prepared by both the *in-situ* and the *ex-situ* approach [15]–[22].

Another important point besides the selection of the best superconducting film, is to use a fabrication technique that allow a transfer of the obtained results to the long-length production. It was demonstrated, in our previous work, that the use of the chemical solution deposition (CSD) is an appropriate technique for the preparation of high-quality YGBCO-BHO films on buffered metallic tapes [23]. The CSD method which is based in the use of chemical solution as precursors for the growth of the final films, is a low-cost scalable and technique that was extensively investigated in the preparation of CCs [24]–[27].

This work is a continuation of our recent publication in which we showed that YGBCO-BHO films can be grown Ni5W substrates with remarkable superconducting properties [23]. In

P. Cayado, M. Erbe, J. Hänisch, and B. Holzapfel are with the Institute for Technical Physics (ITEP), Karlsruhe Institute of Technology (KIT), 76344 Eggenstein-Leopoldshafen, Germany (e-mail: pablo.cayado@kit.edu).

H. Rijckaert and I. Van Driessche are with the Department of Chemistry, Ghent University, SCRiPTS, 9000 Ghent, Belgium.

T. Thersleff is with the Department of Materials and Environmental Chemistry, Stockholm University, SE-106 91 Stockholm, Sweden.

this case we focused in study the microstructure of these films and its relationship with the critical current densities  $J_c$  values obtained by transport measurements.

## II. EXPERIMENTAL DETAILS

The TFA solutions used in this work were prepared following the protocol reported in Ref. [6]. In summary, this is a 1.5 molar solution (over all cations) with a 1:2:3 ratio of *RE*, Ba and Cu dissolved in dry methanol, where *RE* consists of  $(1-x)$  parts Y and  $x$  parts Gd.

The YGBCO+12%BHO films of  $\sim 270$  nm thickness were prepared, firstly, by depositing the precursor solutions on 10 mm  $\times$  10 mm pieces of Ni5W tape via spin coating (6000 rpm for 30 s). The fully CSD-buffered Ni5W substrates were provided by Deutsche Nanoschicht GmbH and include a thin (10–12 nm) top layer of CeO<sub>2</sub> on three layers of 100 nm each of La<sub>2</sub>Zr<sub>2</sub>O<sub>7</sub> (LZO) that were deposited on the biaxially textured Ni5W. The pyrolysis and growth processes used in this case were described in detail in Ref. [23].

Crystallographic properties and phase purity were investigated by X-ray diffraction (XRD, *Bruker* D8, CuK $\alpha$ , Bragg-Brentano geometry). In-field transport critical current densities  $J_c(B)$  were determined in 4-point geometry at a *Quantum Design* Physical Property Measurement System (PPMS, 14 T). For this, 100  $\mu$ m wide bridges were prepared by photolithography and wet-chemical etching.  $J_c$  was calculated from the  $V(I)$  curves with a criterion of 1  $\mu$ V/cm. The microstructure was investigated via TEM images obtained with a *JEOL* JEM-2200FS (200 kV,  $C_s$ -corrected) on lamellae prepared by FIB in-situ lift-out technique (Omniprobe [28]) and subsequent ion milling. Several TEM modes were used for maximum information: crystallographic data by high-resolution (HR) TEM combined with selected area electron diffraction patterns and structural defects by bright-field (BF) TEM. EDX maps were obtained on a Thermo Fischer Themis TEM equipped with a Chem-STEM EDX detector in the Super-X geometry and operated at 300 kV in Cs-corrected STEM mode. The data were processed in the Velox software package.

## III. RESULTS AND DISCUSSION

According to the  $\theta$ - $2\theta$  scans displayed in Fig. 1, it is concluded that there is a strong tendency for the growth of *c*-axis oriented grains since intense (00 $l$ )YGBCO reflections for all films are present. Considering that the (005) reflection of YBCO and GdBCO have similar theoretical intensities, another significant point to consider is that the intensity of this reflection increases with  $x$  indicating that the REBCO phase formation is preferred for larger  $x$  [23]. Furthermore, reflections like ( $h00$ )YGBCO or (103)YGBCO related to *a*-*b* or randomly oriented grains, respectively, are not observed except for an almost negligible (200) peak in the YBCO film. On the other hand, we also observed that the intensity of the reflections associated to BaCeO<sub>3</sub> (BCO), a product of the reaction of the CeO<sub>2</sub> top buffer layer with the Ba from the REBCO matrix, seems to decrease with Gd content  $x$ . This could also cause a reduction in the (00 $l$ )YGBCO intensities since the Ba used to form BCO is not available to form YGBCO anymore.

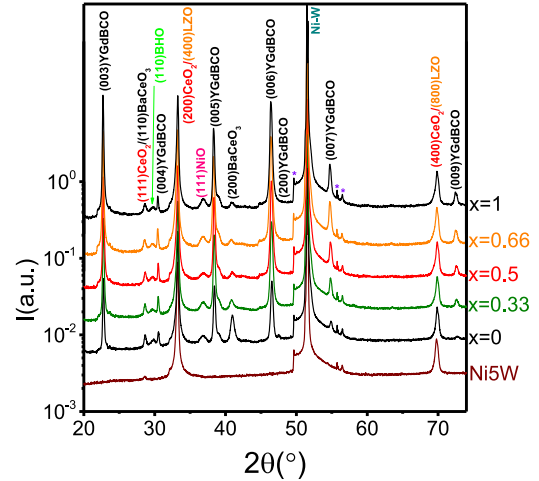


Fig. 1.  $\theta$ - $2\theta$  scans of  $Y_{1-x}Gd_xBa_2Cu_3O_7+12\%BHO$  films on Ni5W substrates. The peaks marked with \* come from the experimental setup.

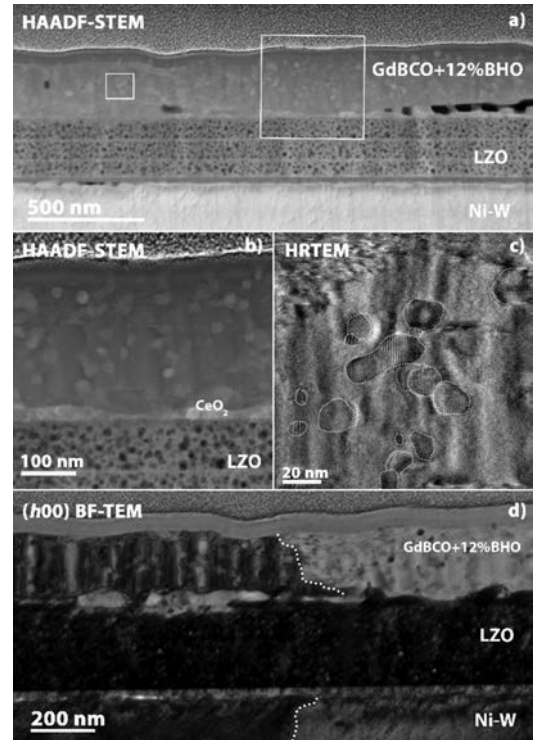


Fig. 2. Microstructure of the GdBCO+12%BHO film on CeO<sub>2</sub>/LZO/Ni5W observed in TEM images: (a) HAADF-STEM cross-sectional overview, (b) higher magnification of (a) at indicated region, (c) HRTEM image of randomly oriented BHO and Gd<sub>2</sub>O<sub>3</sub> particles embedded in the GdBCO matrix, (d) cross-sectional BF-TEM image taken with a diffraction vector  $\vec{g} = (100)$  resolving in-plane misorientation of  $\sim 5^\circ$  between two GdBCO grains.

The microstructure of the films is exemplarily shown with cross-sectional TEM images of the GdBCO+12%BHO, Fig. 2. The GdBCO film appears dense and with rather homogeneous thickness on top of the CeO<sub>2</sub>-covered tri-layer of LZO, Fig. 2(a) and (b). The CeO<sub>2</sub> buffer layer at the interface is rather inhomogeneous in thickness, probably due to the formation of BaCeO<sub>3</sub> (BCO). Some pores at the interface are visible. These two

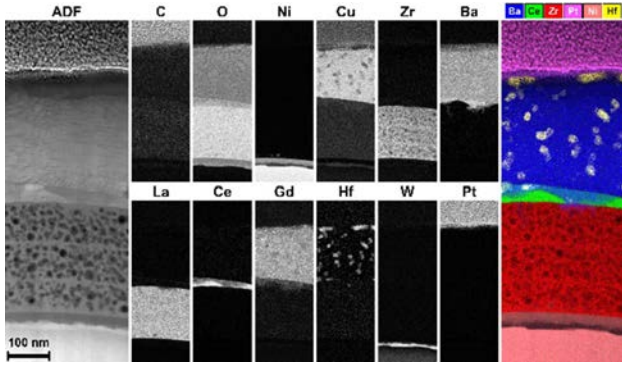


Fig. 3. EDX map of the GdBCO+12%BHO film deposited on CeO<sub>2</sub>/LZO/Ni5W (same film as shown in Fig. 2).

images also evidence a high density of randomly oriented and homogeneously distributed particles. These nanoparticles (NPs) are mainly BHO and Gd<sub>2</sub>O<sub>3</sub> which are difficult to distinguish in STEM due to their similar Z contrast. As displayed in Fig. 2(c)), these NPs are, in some cases, partially agglomerate. Their diameter ranges between 15 and 35 nm. The low magnification BF-TEM image taken with a diffraction vector  $\vec{g} = (100)$ , Fig. 2(d)), visualizes a contrast change due to some misalignment of the GdBCO grains. There is a significant contrast change within both the GdBCO film and the Ni-W substrate marked by a white line, which is caused by the misalignment between two adjacent grains of the metallic tape passed on through the buffer layer to the GdBCO film. The resulting in-plane misorientation between the two GdBCO grains is larger than 5°. This in-plane misalignment is typical for Ni-W and was reported before in literature to be one of the main causes for the reduction of  $J_c$  on this kind of substrates, e.g., [29], [30]. The other films have very similar microstructures, except for  $x = 0$ , which contains larger amount of BCO and misoriented grains and (not shown here).

The EDX map of the GdBCO+12%BHO film deposited on CeO<sub>2</sub>/LZO/Ni5W is displayed in Fig. 3. This map confirms what it was shown before if Fig. 2. A quite homogeneous distribution of BHO NPs throughout the thickness of the film is observed. Also, the CeO<sub>2</sub> layer is not homogeneous in thickness due to the reaction with Ba to form BCO at the interface. The composition of the substrate and buffer layers is homogeneous and the expected one.

The improvement in  $J_c$  and pinning force density  $F_p$  due to BHO nanoparticles as well as Gd content  $x$  is clearly seen in Fig. 4. Due to the pinning effect of the BHO NPs,  $J_c$  of the nanocomposites is significantly larger than the pristine films (open symbols). The advantages of higher Gd content  $x$  (colored symbols) in contrast to the YBCO films (black) is apparent. This improvement is due to both the higher  $T_c$  values as well as better phase formation [23]. The accommodation field  $H^*$  at 77 K (here defined as  $J_c(H^*) = 0.9J_c^f$ ) with values of  $\sim 85$  mT are much larger for all YGBCO+12%BHO films than for the pristine films (here YBCO,  $\sim 25$  mT) and. Also the values of the exponent  $\alpha$  ( $J_c \sim B^{-\alpha}$ ) are lower in the nanocomposites:  $\sim 0.6$  in contrast to  $\sim 1.1$  in the pristine YBCO film (calculated in the range of 85–3000 mT). Furthermore, the YGBCO+12%BHO films

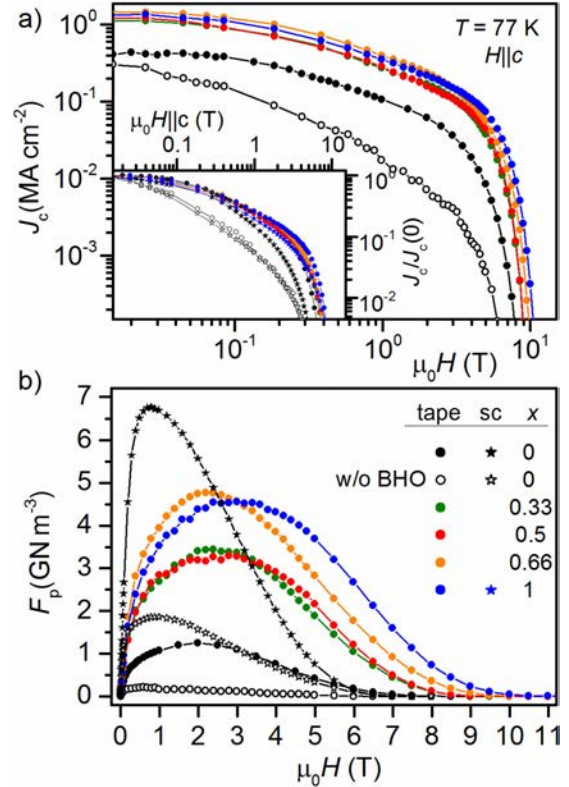


Fig. 4. Transport properties at 77 K of YGBCO+12%BHO films deposited on Ni5W (closed circles) in comparison with pristine YBCO (open symbols) and films on single crystals (stars): (a) magnetic field dependence of  $J_c$  at 77 K, inset: normalized to  $J_c(0)$ , (b) magnetic field dependence of the pinning force density  $F_p$ .

deposited on Ni5W have, in all the cases, lower  $\alpha$  values compared with the same films deposited on single crystals (stars, inset Fig. 4a):  $\sim 0.6$  for the YGBCO+12%BHO films on Ni5W and  $\sim 0.9$  and  $\sim 0.7$  for YBCO+12%BHO and GdBCO+12%BHO films deposited on SrTiO<sub>3</sub>, respectively. This might both be due to reduced  $J_c$  values in low magnetic fields due to grain boundary weak links and increased pinning in high fields due to a larger density of  $c$ -axis-oriented defects such as growth dislocations and twins in the films on Ni5W.

The maximum pinning force densities  $F_p$  at 77 K, Fig. 4(b)), of YGBCO+12%BHO on Ni5W are with 3–5 GN/cm<sup>3</sup> much larger than for pristine YBCO on Ni5W (0.21 GN/m<sup>3</sup> at 0.6 T) and, except for YBCO+12%BHO (data for  $F_p$  at 77 K of GdBCO+12%BHO films in Ref. [6]), even larger than for pristine YBCO on single crystal (1.86 GN/m<sup>3</sup> at 1.0 T). The maximum  $F_p$  value in the film with  $x = 0.66$  on Ni5W is even close to YBCO+12%BHO on single crystal: 4.77 GN/m<sup>3</sup> (at 2.2 T) and 6.77 GN/m<sup>3</sup> (at 0.8 T), respectively. The magnetic fields corresponding to the maximum  $F_p$  values are larger on Ni5W than on single crystals. For example, in GdBCO+12%BHO on Ni5W the maximum is reached at 3.0 T, while the maximum in the YBCO+12%BHO film on single crystal is reached at 1.0 T. This corresponds to the trend in  $\alpha$  discussed above. The pinning forces at 77 K are rather similar for  $x = 0.33$  and  $x = 0.5$ . This may be explained by their very similar  $T_c$  values, which happens

due to experimental scatter. At 77 K, which is still close to  $T_c$ ,  $T_c$  has a major influence on the transport properties.

The improved in-field transport properties of YGBCO+12%BHO on Ni5W are related to their structural features. The high amount of NPs and meandering small-angle grain boundaries observed in TEM improve the pinning performance of these films. The BCO formation is less severe in films with high Gd content, which increases the crystalline quality of the films [23]. For the YBCO films, the formation of BCO is very prominent. This results in the formation of misoriented grains and, consequently, very low  $J_c$  and  $F_p$  values compared to films with larger  $x$ .

All transport  $J_c^{\text{sf}}$  values are  $\sim 25\%$  lower than the corresponding inductively measured values [23]. Presumably, the small yet present porosity in these films is the main reason for this reduction but also the presence of grain boundaries could play a role. The grain boundaries could act as pinning centers causing an improvement of the pinning performances. However, it is very likely that several high-angle grain boundaries (as discussed above) are present in the 100  $\mu\text{m}$  wide bridges which, as weak links, are detrimental for  $J_c^{\text{sf}}$ .

#### IV. CONCLUSION

The influence of the Y/Gd ratio on the film quality has been investigated in the case of  $\text{Y}_{1-x}\text{Gd}_x\text{Ba}_2\text{Cu}_3\text{O}_{7-\delta}\text{-BaHfO}_3$  nanocomposite films prepared by CSD and deposited on Ni5W substrates. Well-textured films free of highly misoriented grains have been achieved for  $x > 0.5$ . The films are dense with homogeneous thickness and a high and homogeneous density of nanoparticles. Both the addition of BHO nanoparticles and higher Gd content  $x$  increase the pinning properties considerably. These results highlight the potential of this approach (CSD of mixed-RE-BCO nanocomposites on Ni5W) for the fabrication of high-quality coated conductors.

#### ACKNOWLEDGMENT

The author acknowledge Deutsche Nanoschicht GmbH for supplying the Ni5W substrates used in this work.

#### REFERENCES

- [1] S. R. Foltyn *et al.*, "Materials science challenges for high-temperature superconducting wire," *Nat. Mater.*, vol. 6, no. 9, pp. 631–642, Sep. 2007.
- [2] A. Goyal, M. P. Paranthaman, and U. Schoop, "The RABiTS approach: Using rolling-assisted biaxially textured substrates for high-performance YBCO superconductors," *MRS Bull.*, vol. 29, no. 08, pp. 552–561, Aug. 2004.
- [3] P. N. Arendt and S. R. Foltyn, "Biaxially textured IBAD-MgO templates for YBCO-coated conductors," *MRS Bull.*, vol. 29, no. 08, pp. 543–550, Aug. 2004.
- [4] M. Murakami *et al.*, "Melt-processed light rare earth element - Ba - Cu - O," *Supercond. Sci. Technol.*, vol. 9, no. 12, pp. 1015–1032, Dec. 1996.
- [5] P. Cayado *et al.*, "Epitaxial superconducting  $\text{GdBa}_2\text{Cu}_3\text{O}_{7-\delta}/\text{Gd}_2\text{O}_3$  nanocomposite thin films from advanced low-fluorine solutions," *Supercond. Sci. Technol.*, vol. 30, no. 12, 2017.
- [6] P. Cayado *et al.*, "Large critical current densities and pinning forces in CSD-grown superconducting  $\text{GdBa}_2\text{Cu}_3\text{O}_{7-x}\text{-BaHfO}_3$  nanocomposite films," *Supercond. Sci. Technol.*, vol. 30, no. 9, 2017, doi: 10.1088/1361-6668/aa7e47.
- [7] M. Erbe *et al.*, "Improved  $\text{REBa}_2\text{Cu}_3\text{O}_{7-x}$  (RE = Y, Gd) structure and superconducting properties by addition of acetylacetone in TFA-MOD precursor solutions," *J. Mater. Chem. A*, vol. 2, no. 14, p. 4932, 2014, doi: 10.1039/c3ta15243j.
- [8] C. Andreouli and A. Tsetsekou, "Synthesis of HTSC  $\text{Re(Y)Ba}_2\text{Cu}_3\text{O}_x$  powders: The role of ionic radius," *Phys. C Supercond.*, vol. 291, no. 3, pp. 274–286, 1997.
- [9] M. S. Islam and R. C. Baetzold, "Atomistic simulation of dopant substitution in  $\text{YBa}_2\text{Cu}_3\text{O}_7$ ," *Phys. Rev. B*, vol. 40, no. 16, pp. 10926–10935, Dec. 1989.
- [10] J. L. Macmanus-Driscoll, "Materials chemistry and thermodynamics of  $\text{REBa}_2\text{Cu}_3\text{O}_{7-x}$ ," *Adv. Mater.*, vol. 9, no. 6, pp. 457–473, 1997.
- [11] M. Erbe *et al.*, "Comparative study of CSD-grown REBCO films with different rare earth elements—Part one: Processing Windows and  $T_c$ ," submitted for publication.
- [12] P. Cayado *et al.*, "Chemical solution deposition of  $\text{Y}_{1-x}\text{Gd}_x\text{Ba}_2\text{Cu}_3\text{O}_{7-\delta}\text{-BaHfO}_3$  nanocomposite films: Combined influence of nanoparticles and rare-earth mixing on growth conditions and transport properties," *RSC Adv.*, vol. 8, no. 74, pp. 42398–42404, Dec. 2018.
- [13] A. V. Narlikar, Ed., *Studies of High Temperature Superconductors*, vol. 49, New York, NY, USA: Nova Science Publishers, 2006.
- [14] Y. Li and Z.-X. Zhao, "Stress-field pinning induced by the lattice mismatch in 123 phase," *Phys. C: Supercond.*, vol. 351, no. 1, pp. 1–4, Mar. 2001.
- [15] J. Gutiérrez *et al.*, "Strong isotropic flux pinning in solution-derived  $\text{YBa}_2\text{Cu}_3\text{O}_{7-x}$  nanocomposite superconductor films," *Nat. Mater.*, vol. 6, no. 5, pp. 367–373, May 2007.
- [16] A. Llordés *et al.*, "Nanoscale strain-induced pair suppression as a vortex-pinning mechanism in high-temperature superconductors," *Nat. Mater.*, vol. 11, no. 4, pp. 329–336, Feb. 2012.
- [17] M. Erbe *et al.*, "BaHfO<sub>3</sub> artificial pinning centres in TFA-MOD-derived YBCO and GdBCO thin films," *Supercond. Sci. Technol.*, vol. 28, no. 11, Nov. 2015, Art. no. 114002.
- [18] P. Cayado *et al.*, "Epitaxial  $\text{YBa}_2\text{Cu}_3\text{O}_{7-x}$  nanocomposite thin films from colloidal solutions," *Supercond. Sci. Technol.*, vol. 28, no. 12, 2015, doi: 10.1088/0953-2048/28/12/124007.
- [19] K. De Keukeleere *et al.*, "Superconducting  $\text{YBa}_2\text{Cu}_3\text{O}_{7-\delta}$  nanocomposites using preformed  $\text{ZrO}_2$  nanocrystals: Growth mechanisms and vortex pinning properties," *Adv. Electron. Mater.*, Sep. 2016, Art. no. 1600161, doi: 10.1002/aelm.201600161.
- [20] S. Engel *et al.*, "Enhanced flux pinning in  $\text{YBa}_2\text{Cu}_3\text{O}_7$  layers by the formation of nanosized BaHfO<sub>3</sub> precipitates using the chemical deposition method," *Appl. Phys. Lett.*, vol. 90, no. 10, Mar. 2007, Art. no. 102505.
- [21] H. Rijckaert *et al.*, "Optimizing nanocomposites through nanocrystal surface chemistry: Superconducting  $\text{YBa}_2\text{Cu}_3\text{O}_7$  thin films via low-fluorine metal organic deposition and preformed metal oxide nanocrystals," *Chem. Mater.*, vol. 29, no. 14, pp. 6104–6113, Jul. 2017.
- [22] H. Rijckaert *et al.*, "Influence of  $\text{Ba}^{2+}$  consumption and intermediate dwelling during processing of  $\text{YBa}_2\text{Cu}_3\text{O}_7$  nanocomposite films," *J. Am. Ceram. Soc.*, Nov. 2018, doi: 10.1111/jace.16228.
- [23] P. Cayado *et al.*, "CSD-grown  $\text{Y}_{1-x}\text{Gd}_x\text{Ba}_2\text{Cu}_3\text{O}_{7-\delta}\text{-BaHfO}_3$  nanocomposite films on Ni5W and IBAD technical substrates," *Nanomaterials*, vol. 10, no. 1, p. 21, 2020, doi: 10.3390/nano10010021.
- [24] X. Obradors and T. Puig, "Coated conductors for power applications: Materials challenges," *Supercond. Sci. Technol.*, vol. 27, no. 4, Art. no. 044003, Apr. 2014.
- [25] X. Obradors *et al.*, "Chemical solution deposition: A path towards low cost coated conductors," *Supercond. Sci. Technol.*, vol. 17, no. 8, pp. 1055–1064, Aug. 2004.
- [26] X. Obradors *et al.*, "Progress towards all-chemical superconducting  $\text{YBa}_2\text{Cu}_3\text{O}_7$ -coated conductors," *Supercond. Sci. Technol.*, vol. 19, no. 3, pp. S13–S26, Mar. 2006.
- [27] T. Izumi *et al.*, "Progress in development of advanced TFA-MOD process for coated conductors," *Phys. C: Supercond. its Appl.*, vol. 463, pp. 510–514, 2007.
- [28] M. Van Zele *et al.*, "Thickness characterization toolbox for transparent protective coatings on polymer substrates," *Materials (Basel)*, vol. 11, no. 7, p. 1101, Jun. 2018, doi: 10.3390/ma11071101.
- [29] R. Hühne *et al.*, "Preparation of coated conductor architectures on Ni composite tapes," *Supercond. Sci. Technol.*, vol. 20, no. 7, pp. 709–714, Jul. 2007.
- [30] P. Pahlke *et al.*, "Local orientation variations in YBCO films on technical substrates—A combined SEM and EBSD study," *IEEE Trans. Appl. Supercond.*, vol. 26, no. 3, pp. 1–5, Apr. 2016.

## Repository KITopen

Dies ist ein Postprint/begutachtetes Manuskript.

Empfohlene Zitierung:

Cayado, P.; Rijckaert, H.; Thersleff, T.; Erbe, M.; Hanisch, J.; Van Driessche, I.; Holzapfel, B.  
[Improved Performance of CSD-Grown  \$Y\_{1-x}Gd\_xBa\_2Cu\_3O\_{7-x}\$ -BaHfO<sub>3</sub> Nanocomposite Films on Ni5W Substrates.](#)

2020. IEEE transactions on applied superconductivity, 30  
[doi: 10.554/IR/1000105797](#)

Zitierung der Originalveröffentlichung:

Cayado, P.; Rijckaert, H.; Thersleff, T.; Erbe, M.; Hanisch, J.; Van Driessche, I.; Holzapfel, B.  
[Improved Performance of CSD-Grown  \$Y\_{1-x}Gd\_xBa\_2Cu\_3O\_{7-x}\$ -BaHfO<sub>3</sub> Nanocomposite Films on Ni5W Substrates.](#)

2020. IEEE transactions on applied superconductivity, 30 (4), Article no: 6600204.  
[doi:10.1109/TASC.2020.2966429](#)

Lizenzinformationen: [KITopen-Lizenz](#)